Tuning electron transport through molecular junctions by chemical modification of the molecular core: First-principles study

Shigeru Tsukamoto,[*] Vasile Caciuc, Nicolae Atodiresei, and Stefan Blügel

Peter Grünberg Institut and Institute for Advanced Simulation, Forschungszentrum Jülich and JARA, D-52425 Jülich, Germany

The unique versatility of the electronic structures of organic molecules can be potentially utilized to engineer single-molecular electronic devices with specific functionalities. Here, we report on how the electronic structures and the transport properties of molecular junctions containing a π-conjugated terephthalic acid molecule in a scanning tunneling microscopy (STM) configuration can be tuned by modifying their chemical composition at a single-atom level. More specifically, this strategy implies (i) to change the molecular core through a chemical functionalization process and (ii) to modify the chemical nature of the STM-tip-apex atom. In this respect, our first-principles calculations of the electronic structures and the corresponding electron transport reveal that by the insertion and increase of the number of N atoms in the six-membered benzenelike aromatic ring, the electron transmission at the Fermi level increases. However, the calculated electron transmission at the Fermi level does not depend significantly on the specific position of the N atom in the aromatic ring. Nevertheless, when the tip-apex atom is changed from Cu to W, the electron transmission of the molecular junction significantly changes in an energy range above the Fermi level.

I. INTRODUCTION

Since the first suggestion of the nanoscale device based on organic molecules, i.e., single-molecular rectifier has been designed theoretically by Aviram and Ratner,[1] even at present molecular electronics is still an exciting field from the perspective that various types of electronic functionalities can be potentially realized only by single molecules due to their unique electronic structures. Therefore, in the last decade special attention was paid to investigate organic molecular junctions to understand their fundamental physics and to explore their applications.[2]

In particular, to bring single-molecular electronic devices into reality, it is absolutely imperative to comprehend electronic structures not only of the isolated molecules but also of the molecular junctions assembled from a single molecule sandwiched between metal electrodes. Moreover, electron transport properties of the molecular junctions must be also understood to evaluate their potential use in functional electronic devices. In consequence, an enormous effort has been devoted to investigate the fundamental physics of single-molecular junctions including their electronic structures and transport properties from both experimental and theoretical points of view.[3] For instance, Venkataraman *et al.* have adopted a conformational modification approach to experimentally investigate the systematic change in electron transport through single molecules containing two planar units such as biphenyl/bithiophen, and revealed that the twist angle between the two benzene/thiophene rings strongly affects the conductance.[4] Reddy *et al.* have also reported the systematic change in the thermopower of thiol-terminated oligophenyl as the function of the molecular length[5] (for a review see, for example, Ref. [6]). Additionally, the dependence of the electrical conductance on the nature of the anchoring group of oligoynes of different lengths has been recently addressed.[7]

So far, our research group has suggested that a carboxylate group can be a promising candidate to anchor organic molecules on the Cu(110) surface[8,9] similarly to the thiolate group, which is well known to anchor organic molecules on the Au(111) surface.[10,11] Recently, we have experimentally and theoretically studied several single π-conjugated organic molecules such as carboxylates chemisorbed on the Cu(110) surface, and pointed out that the electronic structure of a prototype terephthalic-acid ($C_8H_6O_4$, denoted also as TPA) molecule can be specifically tuned by a systematic modification at a single-atom level of the chemical composition of its molecular core given by a benzenelike aromatic ring.[12] In addition to these studies, we have also performed the systematic investigation on the electron transport properties of a symmetric TPA molecular junction in a break-junction configuration and found that the electron transmission through this molecular junction can be precisely tuned by a chemical modification approach, that is, replacing the C atom in the anchoring carboxylate groups (COO) through a more electronegative atom such as N or a less electronegative one like B.[13]

In this study we have extended our previous research to analysis of the electron transport in single-molecular junction integrated in a scanning tunneling microscopy (STM) configuration. Since its invention,[14] the STM, especially multiprobe STM, had become the surface science tool of choice to characterize the topography of adsorbate-surface systems and even to investigate their electronic structure by means of scanning tunneling spectroscopy (STS).[15] In our previous works,[8,9,12] STM and STS played a key role in understanding the electronic structures of organic molecules chemisorbed on the Cu(110) surface. Therefore, the theoretical electron-transport studies that are comparable to STM measurements are absolutely requisite for a detailed understanding of the transport properties measured from single-molecular junctions in a STM configuration. Note that in a STM configuration, single-molecular junctions have an asymmetric structure composed of a substrate electrode, an organic molecule adsorbed on it, a vacuum gap, and a tip electrode.

In this study, adopting single-molecular junction systems in a STM configuration, where a tip electrode scans above the organic molecule chemisorbed in an upright geometry on the Cu(110) surface as employed in the previous work,[12] we present a systematic investigation on the electronic structures and the ballistic electron-transport properties of such single-molecular junctions. Our systematic study on the single-molecular junctions starts (i) from a prototype TPA molecule, (ii) replaces a CH group in the aromatic ring of the molecular core with a more electronegative N atom, and (iii) increases the number of the N atoms in the ring by a further CH replacement. In addition to the modification of the chemical structure of the TPA molecule, the vacuum-gap width between the top of an organic molecule and the surface of a tip electrode is also changed to examine the variation of the electron transport properties from the contact condition to the tunnel condition.

Our first-principles calculations provide a precise recipe on how to specifically control electron transmission at the Fermi level of the single-molecular junctions (i) by modifying chemical composition of the molecular core and (ii) by changing geometrical separation between the organic molecule and the STM tip. Moreover, an important outcome of our first-principles study is that the exchange of the atom at the tip apex induces drastic changes in the electron transmission at the Fermi level. Overall, our results point out the importance of the chemical and geometrical fine tuning of molecular junctions on their electronic transport properties.

This paper is organized as follows: In the next section, we describe the computational methods used in this study and present molecular junction models employed in this work. In Sec. III, we analyze the electronic structures and electron transmissions of the STM junction systems incorporating the prototype TPA molecule and the chemically functionalized ones, while in Sec. IV we summarize the results obtained in our systematic theoretical investigation.

II. CALCULATION METHOD AND MODEL

All calculations presented in this paper are performed within the framework of the density functional theory (DFT).[16] To determine the electronic ground states of the organic molecular junction systems in a STM configuration, we have used an electronic-structure calculation code[17] based on the real-space finite-different formalism,[18] in which the projector-augmented-wave pseudopotentials method proposed by Blöchl[19] is incorporated to describe the interaction between valence electrons and a nucleus, and the exchange-correlation interaction is treated by the local density approximation (LDA).[20] Our first-principles electronic-structure calculation method enables us to determine the self-consistent electronic ground states of target systems with a high degree of accuracy by means of the timesaving double-grid technique.[21]

In the computations of the electron transmissions through the molecular junctions, we employ a code calculating ballistic electron transport based on the real-space finite-difference formalism[22] in order to keep consistency with the electronic-structure calculations mentioned above. The effective local potential and the pseudopotential parameters, which are determined self-consistently and exported from the electronic-structure calculations, are the input into the electron-transport

code, and hence, the scattering wave functions of electrons inside the molecular junction systems are determined to the given potential in a non-self-consistent manner. It has been reported that the non-self-consistent procedure is just as accurate within the linear response regime but significantly more efficient than performing self-consistent expensive computations on a scattering wave basis.[23] Electron transmission $G(E)$ is evaluated by means of the Landauer-Büttiker formula,[24] i.e.,

$$G(E) = G_0 T(E) = G_0 \sum_{i,j} T_{ij}(E). \tag{1}$$

G_0 is the quantized conductance, and $G_0 = 2e^2/h$, where e is the electron charge and h is Planck's constant. Here, T_{ij} is the transmission probability of the electrons flowing from the ith channel in an electrode to the jth channel in another electrode, and is obtained from scattering wave functions by means of the channel decomposition technique.[25]

It is important to keep in mind that the use of the LDA functional in DFT calculations may result in the overestimation of electron transmission at the Fermi level because of the underestimation of band gaps.[26] However, on the other hand, LDA-based transport calculations are well known to give a reliable insight into the qualitative trends of electron transport properties in molecular junctions.[27]

Figure 1 shows a schematic representation of the computational model employed in our first-principles study. The TPA molecule, which has a benzenelike aromatic ring as the molecular core between two carboxylic groups, chemisorbs on the Cu (110) modeled by three Cu(110) layers via two carboxylate-Cu anchoring bonds,[28] and is standing perpendicular to surface, which acts as an electrode of the two-terminal molecular junction. Another electrode is made up of two Cu(110) layers and an apex atom on it, and is placed at a few Å above the carboxylic group of the TPA molecule at the vacuum interface, so as to include a vacuum gap between them. Thus, an asymmetric single-molecular junction in a STM configuration is formed.
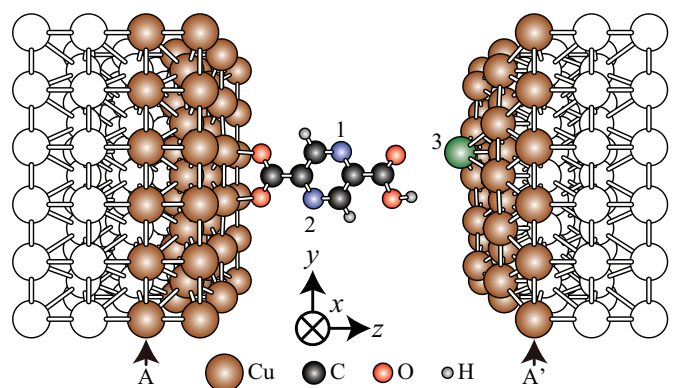

FIG. 1. (Color online) A schematic representation of the geometrical model employed in this work. An organic molecule is chemisorbed in an upright configuration on the Cu(110) surface, and a STM tip is placed on the top of the molecule. The atoms labeled as 1, 2, and 3 are replaced by other atoms as described in Table I. For each electrode, four Cu(110) bulk layers depicted as white balls are approximated with a jellium model.

To evaluate the influence of the vacuum gap on the electron transport properties of the junctions, we have also changed the distance between the organic molecule and the STM tip, as follows. The distance between the Cu(110) layers indicated by A and A' in Fig. 1, $d_{A-A'}$, is set to be 15.87 Å, 16.87 Å, and 19.87 Å so that the distance between the tip-apex atom and the nearest O atom before geometry optimization is to be 2 Å, 3 Å, and 6 Å, respectively. Then the whole atomic structure except for the outermost Cu(110) layer indicated by A and A' in Fig. 1 is optimized. The optimized distance between the tip-apex atom and the O will be discussed later. Hereafter, the systems optimized for $d_{A-A'} = 15.87$ Å, 16.87 Å, and 19.87 Å are referred to as Short, Middle, and Long, respectively. We have assumed periodic boundary conditions for the directions parallel to the substrate surface.[29]

Since the electron transport calculation method employed in this work requires a uniform background positive charge distribution at around the supercell boundaries in the z direction, the four bulklike Cu(110) layers in each electrode (see the white balls in Fig. 1) are replaced by jellium. In other words, the surface of each Cu electrode is represented by atomic Cu(110) layers and the bulk is approximated by a jellium model.[30] In the jellium approximation, the only parameter needed to be specified is the Wigner-Seitz radius, which is set to 0.64 Å (1.21 bohrs). Note that such use of jellium approximation forms an artificial interface between an atomic layer and the jellium surface, which may raise unphysical influence on electronic structure and transport properties. In this work, by comparing the electronic structures of the systems with and without jellium approximation, we have confirmed that such unphysical influence is negligible.

The single-atom-level modification of the chemical composition of the starting TPA molecular junction is summarized in Table I. To investigate the influence of more electronegative N atoms as compared to the C ones on the electronic structure and the electron transport feature of the molecular junction, we have increased the number of N atoms contained in the aromatic ring at the molecular core, as TPA molecule (without N atoms), pyridinedicarboxylic acid (Py) molecule with an N atom, and pyrazinedicarboxylic acid (Pz) molecule with two N atoms. Since there are two possible positions for one N atom in the Py molecule as described in Table I, we refer to them as Py(sub.) and Py(tip), and examine both systems for the difference in the electronic structures and the transport

TABLE I. Atoms indicated as 1, 2, and 3 in Fig. 1 are replaced by other atoms to carry out the systematic investigation on the change of the electron transport features of the molecular systems considered in our study. Besides this the optimized distances between the tip-apex atom and the nearest O atom are listed in the unit of Å for the three tip-sample separations Short, Middle, and Long.

1	CH	CH	N	N
2	CH		N	CH	N
3	Cu	W	Cu	Cu	Cu
	TPA(Cu)	TPA(W)	Py(sub.)	Py(tip)	Pz
Short	1.97	1.96	1.98	1.98	1.99
Middle	3.20	2.09	3.27	3.29	3.33
Long	6.37	6.36	6.39	6.43	6.45

properties. Since in the STM experiments the W is often used as tip material, we have also exchanged only the apex atom of the tip electrode with W atom and compared the optimized geometries, the electronic structures, and the electron transport properties with the results obtained for a Cu tip. Hereafter, the molecular junction with a Cu atom and a W atom at the tip apex are referred to as TPA(Cu) and TPA(W), respectively. In Table I, the optimized distance between the tip-apex atom and the nearest O atom in each system is also listed for the three tip-sample separations Short, Middle, and Long.

III. RESULTS AND DISCUSSION

Firstly, we analyze the electronic structure and the corresponding electron transport behavior of the TPA(Cu), Py(sub.), and Pz molecular junctions, each of which containing 0, 1, or 2 N atom(s) in the aromatic rings [see Table I]. Figure 2(a) shows the local density of states (LDOS) $N(E)$ at the molecular site, which are evaluated as

$$N(E) = \int_{\text{Mol.}} \sum_i |\psi_i(\boldsymbol{r})|^2 f(E - \varepsilon_i) \mathrm{d}\boldsymbol{r}, \qquad (2)$$
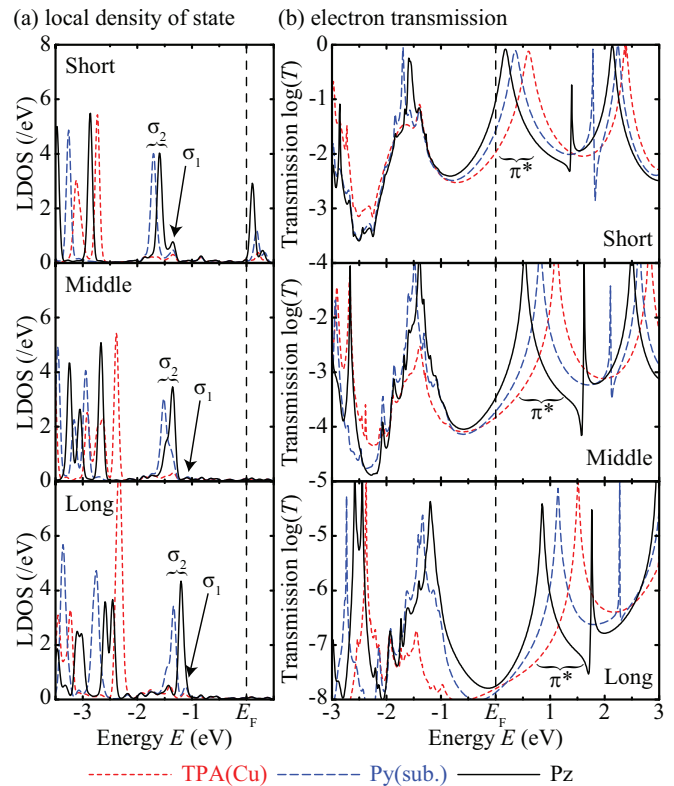

FIG. 2. (Color online) Local density of states (LDOS) at the molecular site and the corresponding electron transmissions of the molecular junctions of the tip-sample separations Short, Middle, and Long. The red short-dashed, blue long-dashed, and black solid curves represent the junction systems of the TPA molecule with Cu tip apex, the Py molecule with N atom at the substrate side, and the Pz molecule, respectively. The vertical dashed line indicates the Fermi level of the systems. Note that the scales of the ordinate in the panel (b) are adjusted so that the curves fit into each graph frame.

where ε_i and ψ_i are the eigenenergy and the wave function of the ith state, respectively, and the integration is carried out over a volume containing only the organic molecule. $f(E - \varepsilon_i)$ is a broadening function with the center at the energy of ε_i. In this work, we have chosen a Gaussian function for the broadening function.[31]

For the Cu-terminated tip, below the Fermi level the states σ_1 and σ_2 with a σ-like molecular character (i.e., they involve the in-plane p_y- and p_z-like atomic orbitals) are present at the molecular site. Although the σ_1 states do not significantly change their energetic position for all three molecular junctions at each tip-sample separation, the position in energy of the σ_2 states is specific for each molecular junction. We also note that the peak position of the σ_2 state for the Pz molecular junction is higher in energy (closer to the Fermi level) than that for Py(sub.) molecular junction for all tip-sample separations. This observation suggests that the presence of N atom in the aromatic ring pushes the σ_2 state to higher energy as already noticed in literature.[32] Besides this, when changing the number of the N atoms the σ_1 and σ_2 states behave in a similar way with the case of the same molecules on the Cu(110) surface in the absence of the STM tip.[12]

Moreover, the height of the LDOS peak of the σ_2 state for the TPA molecular junction is significantly smaller than those for the other two junctions. This feature can be understood from the spatial distributions of the σ_2 wave functions, which are depicted in Fig. 3. In the cases of the molecular junctions containing N atom(s), one can easily see the hybridization of the σ_1 and σ_2 electronic states with those of the Cu(110) surface. In particular, the σ_1 state is mainly localized at the anchoring COO-surface interface while the σ_2 state generally delocalizes over the whole molecular plane. However, in the case of the TPA(Cu) molecular junction the σ_2 state is mainly

(a) σ_2 TPA(Cu) Middle   (b) σ_1 TPA(Cu) Middle

(c) σ_2 Py(sub.) Middle   (d) σ_1 Py(sub.) Middle

(e) σ_2 Pz Middle   (f) σ_1 Pz Middle

FIG. 3. (Color online) Spatial distributions of σ-like wave functions. The six panels present the isosurfaces of the absolute squares of the wave functions marked as σ_1 and σ_2 in Fig. 2(a) for each of the TPA(Cu), Py(sub.), and Pz molecular junctions for the tip-sample separation Middle.

localized at the carboxylate group like the σ_1 state. The fact that the σ_1 states are basically localized at the molecule-surface interface for all three molecular junctions implies that their contribution to the junction electronic structure is similar as depicted in Fig. 2.

The large height of the σ_2 LDOS peak, implying an extension of the electronic state over molecule as discussed above, is also reflected in electron transmission curves. Figure 2(b) shows the electron transmissions of the TPA(Cu), Py(sub.), and Pz molecular junctions for the three tip-sample separations. The transmission peaks corresponding to the σ_2-like states are observed in the energy range from -2.0 eV to -1.0 eV. It is easily seen that the transmission peaks for the molecular junctions containing N atom(s) are at least one order of magnitude larger than those for the TPA molecular junction without N atom. This can be interpreted as follows: In the case of the TPA(Cu) molecular junction, the molecular core acts as a tunnel barrier for the electrons passing through the σ_2 state since it has no weight at the molecular core. On the contrary, in the case of the other two molecular junctions, the organic molecule appears as a conductor for the electrons passing through the σ_2 state since it is extended over the whole molecule.

Above the Fermi level, the transmission peaks labeled as π^* change more drastically as a function of the energy when changing both the number of N atom(s) and the tip-sample separation. To illustrate this effect, one can observe that in each panel of Fig. 2(b) the first transmission peak above the Fermi level moves to lower energies when changing the organic molecule from TPA(Cu) to Py(sub.) and Pz, suggesting that the lowest unoccupied state of the molecular junction lowers in energy by increasing the number of N atom(s) in the aromatic ring. This behavior is also in good agreement with that observed for molecule-surface systems without the STM tip.[12]

When the tip-sample separation is decreased, the transmission peak π^* at ≈ 1.0 eV for the tip-sample separation Long approaches to the Fermi level, and the energy gap between transmission peaks across the Fermi level becomes smaller. This trend is consistent with the scanning tunneling spectroscopy measurements performed in our previous work.[9] The shape of the transmission peak π^* is also found to become broader as reducing the tip-sample separation. In consequence, the tail of the transmission peak starts to contribute more significantly to the electron transmission at the Fermi level, and the transmission peaks reach a quantized value in the contact limit at the tip-sample separation Short.

Next, we investigate how a different position of the N atom in a Py molecule affects the electronic structure and the electron transmission of the corresponding molecular junction. Therefore, we compare the Py(sub.) and Py(tip) molecular junctions, each of which having the N atom at the substrate side or the tip side in the aromatic ring, as seen in Fig. 1 and Table I. Figure 4 presents the LDOS of these two molecular junctions. Interestingly, by increasing the tip-sample separation, the σ_2-like state of the Py(tip) molecular junction becomes closer to the Fermi level than that of the Py(sub.) molecular junction, i.e., the σ_2 state of Py(tip) is lower and higher in energy than the σ_2 state of Py(sub.) for the tip-sample separations Short and Long, respectively.

The different change in the energetic positions of the two σ_2 states can be understood as follows: As depicted in Figs. 3(c)
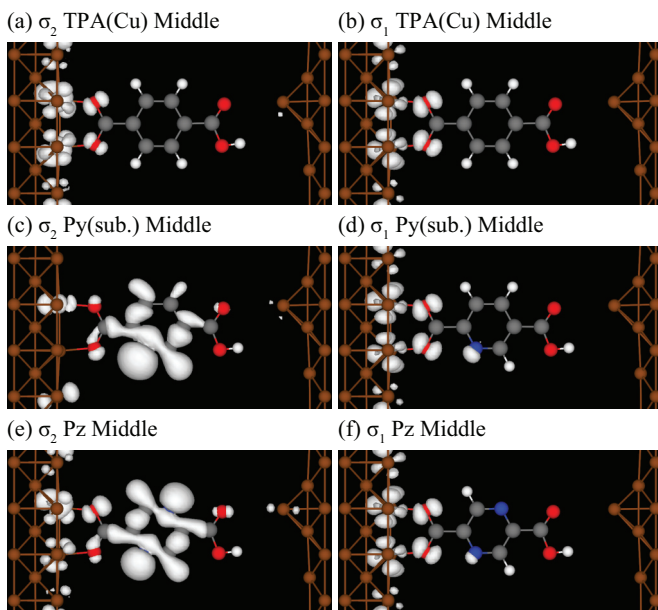
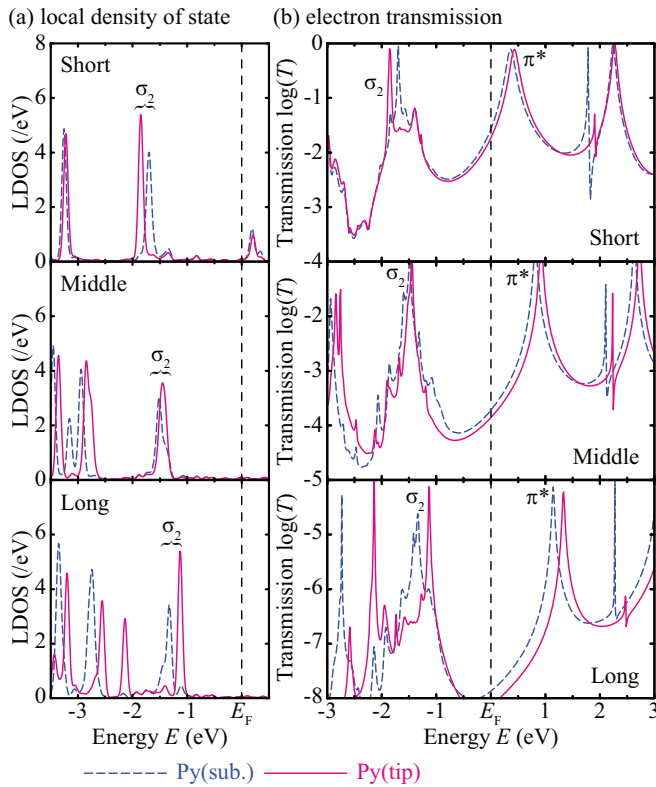(a) local density of state　　(b) electron transmission

FIG. 4. (Color online) Local density of states at the molecular site and the corresponding electron transmissions of the molecular junctions of the tip-sample separations Short, Middle, and Long. The blue dashed curve represents the junction system of the Py molecule with a N atom at the substrate side as plotted in Fig. 2, and the magenta solid curve represents that of the Py molecule with a N atom at the tip side. The vertical line indicates the Fermi level of the systems. Note that the scales of the ordinate in the panel (b) are adjusted so that the curves fit into each graph frame.

and 5(a), the σ_2 state of the Py(tip) junction is closer to the tip than that of Py(sub.), because these σ_2 states are mainly localized around the N atom. This fact implies that the σ_2 state of the Py(tip) junction is affected by the tip approach/retraction more sensitive than that of the Py(sub.) junction. Therefore, by decreasing the tip-sample separation, the σ_2 states are stabilized due to the interaction with the tip, and hence, the energetic position of the σ_2 state of the Py(tip) junction moves to more lower energies than that of the Py(sub.) junction.

The shift in energy of the σ_2 states is also reflected in the electron transmission curves as seen in Fig. 4(b). More
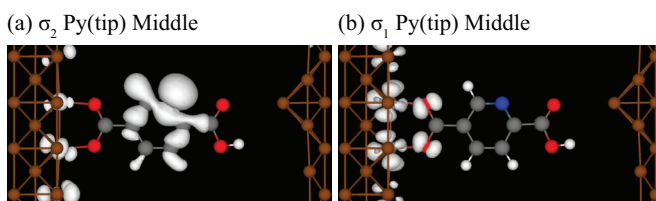

FIG. 5. (Color online) Spatial distributions of σ-like wave functions. The two panels present the isosurfaces of the absolute squares of the wave functions marked as σ_1 and σ_2 in Fig. 4(a) for the Py(tip) molecular junction for the tip-sample separation Middle.

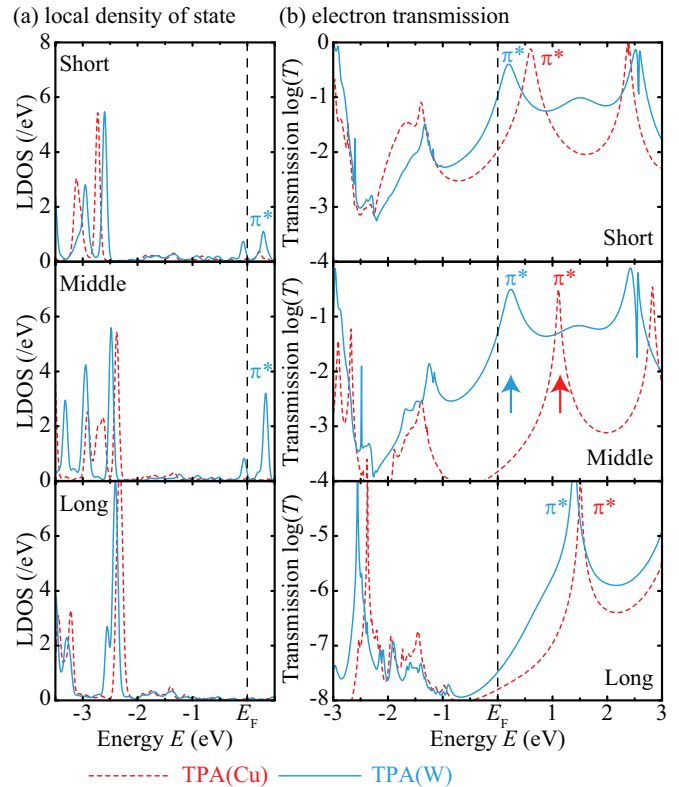

(a) local density of state　　(b) electron transmission

FIG. 6. (Color online) Local density of states at the molecular site and the corresponding electron transmissions of the molecular junctions of the tip-sample separations Short, Middle, and Long. The red dashed curve represents the TPA molecular junction system with a Cu atom at the tip apex as plotted in Fig. 2, and the cyan solid curve represents that with a W atom at the tip apex. The vertical line indicates the Fermi level of the systems. Note that the scales of the ordinate in the panel (b) are adjusted so that the curves fit into each graph frame.

specifically, the transmission peak corresponding to the σ_2 state of Py(tip) moves lower in energy, and overtakes that of Py(sub.) as decreasing the tip-sample separation. However, in spite of the different spatial distributions of the σ_2 states [see Figs. 3(c) and 5(a)], the electron transmissions derived from these states are both in the same magnitude, except for the case of the tip-sample separation Long. Besides this, in the energy range above the Fermi level, the energy separation between the transmission peaks of these two Py molecular junctions becomes small. This observation suggests that it would be difficult to distinguish the Py(tip) and Py(sub.) geometries by STM measurement when a tip is nearly in contact with a Py molecule.

Finally, we analyze the influence of the chemical nature of the tip apex on the electronic structure and the electron transmission of single-molecular TPA junction systems, i.e., the TPA(Cu) and TPA(W) systems with a Cu and W atom as the tip apex, respectively. Figure 6(a) presents the LDOS of these TPA molecular junctions. One can clearly see that in comparison with the TPA(Cu) junction, the TPA(W) junction exhibits an additional LDOS peak with a π-like character above the Fermi level in each panel for the tip-sample separations Short and Middle. These unoccupied π^*-like states

(a) relaxed TPA(Cu) Middle   (b) relaxed TPA(W) Middle

(c) π* channel of TPA(Cu) Middle   (d) π* channel of TPA(W) Middle
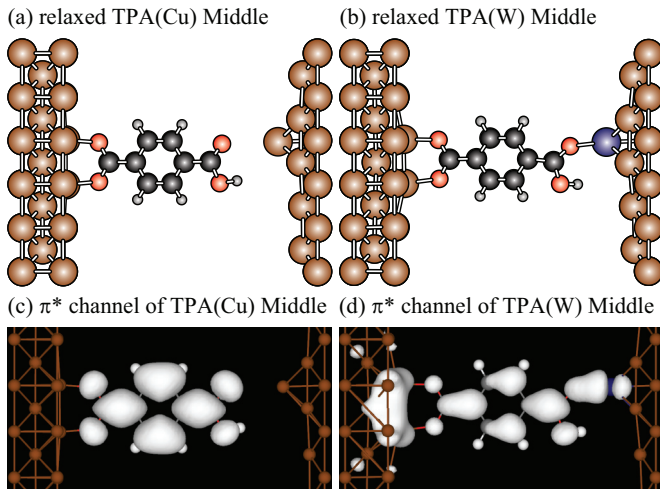

FIG. 7. (Color online) Optimized structures of the TPA molecular junctions in a STM configuration of the tip-sample separation Middle, and spatial distribution of the channel-decomposed wave functions. (a) and (b) show the optimized atomic configurations of the junction systems with Cu and W atom at the tip apex, respectively. (c) and (d) plot the isosurface of the absolute square of the primary eigenchannels contributing to the transmission peaks at the energies indicated by the arrows in Fig. 6(b).

of the TPA(W) junction lead to the transmission peaks at the energy above the Fermi level as seen in the upper two panels in Fig. 6(b), which have the same characteristic to the transmission peak at the $+1.5$ eV for the tip-sample separation Long.

Although in the case of the TPA(Cu) system the π^* transmission peak above the Fermi level monotonously moves to lower energies side and becomes broad gradually when decreasing the tip-sample separation, in the case of the TPA(W) system the corresponding transmission peak remains at the same energy for the tip-sample separation Short and Middle where it is also significantly broadened while it is sharp at the tip-sample separation Long. This different behavior of the transmission peaks can be understood from the optimized geometries of the two systems. Figures 7(a) and 7(b) show the optimized atomic configurations of the organic molecules for the TPA(Cu) and TPA(W) molecular junctions, respectively. One can easily see a significant difference between these relaxed geometries, namely in the case of the TPA(W) junction the W apex atom forms a chemical bond with the underlying O atom at the tip-sample separation Middle, also as listed in Table I. This fact can be explained from the general trend of covalent-bond radii,[33] i.e., a W atom has larger covalent-bond radius than a Cu atom. For the TPA(W) junction system with the tip-sample separation Middle, the energy gain from the formation of the chemical bond between the W and O atoms overcomes the energy required to distort TPA molecule and Cu(110) substrate. This effect can be observed in particular for the carboxylic group at the tip side and for the Cu atoms anchoring of the TPA molecule, as seen in Fig. 7(b). In consequence, this bonding state stabilizes the π^*-like electronic state above the Fermi level, and exhibit the larger electron transmission at the Fermi level in comparison with the TPA(Cu) junction system for the tip-sample separation Middle.

We have also performed the eigenchannel decomposition of the scattering wave functions injected from the electrode at the substrate side. Figures 7(c) and 7(d) depict primary eigenchannels contributing to the transmission peaks at $+0.25$ and $+1.12$ eV indicated by the arrows in Fig. 6(b). The primary eigenchannels both have π^*-like characteristic and localize at the molecular site because the injected waves at the energies resonate with the π^* molecular states. These π^*-like characters of the wave functions at the molecular site are well consistent with our previous work.[13] One can see in the spatial distribution of the eigenchannel waves that the electron-transmission channel of TPA(Cu) junction system for the tip-sample separation Middle is blocked at the vacuum gap between the TPA molecule and the Cu-terminated tip, and that of the TPA(W) junction system for the same tip-sample separation bridges over the gap to reach the W atom. Now, this fact raises the question why the electron transmission values at the energies indicated by the arrows in Fig. 6(b) are almost the same, even though the primary eigenchannel shown in Fig. 7(d) bridges over the gap between the molecule and the tip and the other one shown in Fig. 7(d) does not. Our detailed analysis on the electron flow through the transmission channels answers this question, that is, this is due to the difference in the specific region in the molecular junction where electron backscattering occurs. In the case of the TPA(Cu) junction, it is clearly seen that electron backscattering occurs at the vacuum gap between the molecule and the tip. On the other hand, in the case of the TPA(W) junction, electron backscattering takes place at the interface between the W atom and the Cu (110) substrate.

For the tip-sample separation Middle, the transmission curves of both junction systems are significantly different from each other. Based on the assumption that the electronic structure and electron transmission do not change as long as a sufficiently small bias voltage is applied, we can expect that in the TPA(W) junction system the current flow drastically changes as the energy window due of the bias voltage includes the π^* transmission peak above the Fermi level, while in the TPA(Cu) junction system such a drastic change in the current flow does not occur because the transmission peak is still far away from the Fermi level. In this way, the current-voltage characteristics of the two systems are expected to differ from each other significantly.

IV. CONCLUSION

To conclude, in this theoretical study we have presented a systematic investigation on how electronic structures and electron transmissions can be tuned by changing at a single atom level the chemical composition of molecular junctions in a STM configuration. More precisely, by replacing a CH group in the aromatic ring of a TPA molecule with an electronegative N atom and by increasing their number, the transmission properties can be specifically tailored as well as the electronic structure of the molecular junction system. By changing the tip-sample separation, we have observed the transition between contact and tunnel transport regimes with a monotonous shift of the σ and π transmission peaks. We have also demonstrated that by changing the chemical nature of the tip apex from Cu

to W, the optimized geometry of the TPA molecular junction changes drastically, and consequently the electron transport property is also strongly modified. Therefore, one can conclude that the chemical modification (functionalization) approach employed in this work is one of the practical ways to investigate systematic change in the electronic properties of nanostructure similarly to the conformational modification approach.[4] The knowledge obtained from this study can be further used toward an efficient design of future molecular electronic devices with specific and desired functionalities as well as a fundamental understanding of the basic process that describes the electron transport in single-molecular junctions.

*Corresponding author: s.tsukamoto@fz-juelich.de

[1] A. Aviram and M. A. Ratner, Chem. Phys. Lett. **29**, 277 (1974).

[2] C. Joachim, J. K. Gimzewski, and A. Aviram, Nature (London) **408**, 541 (2000); A. Nitzan and M. A. Ratner, Science **300**, 1384 (2003); L. Lafferentz, F. Ample, H. Yu, S. Hecht, C. Joachim, and L. Grill, *ibid.* **323**, 1193 (2009); J. S. Seldenthuis, F. Prins, J. M. Thijssen, and H. S. J. van der Zant, ACS Nano **4**, 6681 (2010).

[3] S. V. Aradhya and L. Venkataraman, Nat. Nanotechnol. **8**, 399 (2013); S. Quek, L. Venkataraman, H. Choi, S. Louie, M. Hybertsen, and J. Neaton, Nano Lett. **7**, 3477 (2007); E. Lörtscher, J. Ciszek, J. Tour, and H. Riel, Small **2**, 973 (2006); M. Di Ventra, *Electron transport in nanoscale systems* (Cambridge University Press, Cambridge, 2008).

[4] L. Venkataraman, J. E. Klare, C. Nuckolls, M. S. Hybertsen, and M. L. Steigerwald, Nature (London) **442**, 904 (2006); E. J. Dell, B. Capozzi, K. H. DuBay, T. C. Berkelbach, J. R. Moreno, D. R. Reichman, L. Venkataraman, and L. M. Campos, J. Am. Chem. Soc. **135**, 11724 (2013).

[5] P. Reddy, S.-Y. Jang, R. A. Segalman, and A. Majumdar, Science **315**, 1568 (2007).

[6] H. Song, M. A. Reed, and T. Lee, Adv. Mater. **23**, 1583 (2011).

[7] P. Moreno-García, M. Gulcur, D. Z. Manrique, T. Pope, W. Hong, V. Kaliginedi, C. Huang, A. S. Batsanov, M. R. Bryce, C. Lambert, and T. Wandlowski, J. Am. Chem. Soc. **135**, 12228 (2013).

[8] M. C. Lennartz, N. Atodiresei, L. Müller-Meskamp, S. Karthäuser, R. Waser, and S. Blügel, Langmuir **25**, 856 (2009); N. Atodiresei, V. Caciuc, K. Schroeder, and S. Blügel, Phys. Rev. B **76**, 115433 (2007).

[9] M. C. Lennartz, V. Caciuc, N. Atodiresei, S. Karthäuser, and S. Blügel, Phys. Rev. Lett. **105**, 066801 (2010).

[10] M. Di Ventra, S. T. Pantelides, and N. D. Lang, Phys. Rev. Lett. **84**, 979 (2000); J. Nara, W. T. Geng, H. Kino, N. Kobayashi, and T. Ohno, J. Chem. Phys. **121**, 6485 (2004); Y. Egami and K. Yamada, Comput. Phys. Commun. **182**, 103 (2011).

[11] M. A. Reed, C. Zhou, C. J. Muller, T. P. Burgin, and J. M. Tour, Science **278**, 252 (1997); Y. Kim, T. Pietsch, A. Erbe, W. Belzig, and E. Scheer, Nano Lett. **11**, 3734 (2011); D. Q. Andrews, R. P. Van Duyne, and M. A. Ratner, *ibid.* **8**, 1120 (2008); K. Horiguchi, M. Tsutsui, S. Kurokawa, and A. Sakai, Nanotechnology **20**, 025204 (2009); A. Arnold, F. Weigend, and F. Evers, J. Chem. Phys. **126**, 174101 (2007).

[12] V. Caciuc, M. C. Lennartz, N. Atodiresei, S. Karthäuser, and S. Blügel, Nanotechnology **22**, 145701 (2011).

[13] S. Tsukamoto, V. Caciuc, N. Atodiresei, and S. Blügel, Phys. Rev. B **85**, 245435 (2012).

[14] G. Binnig, H. Rohrer, C. Gerber, and E. Weibel, Phys. Rev. Lett. **49**, 57 (1982).

[15] T. Nakayama, O. Kubo, Y. Shingaya, S. Higuchi, T. Hasegawa, C.-S. Jiang, T. Okuda, Y. Kuwahara, K. Takami, and M. Aono, Adv. Mater. **24**, 1675 (2012); C. Wagner, N. Fournier, F. S. Tautz, and R. Temirov, Phys. Rev. Lett. **109**, 076102 (2012); S. Karthäuser, J. Phys.: Condens. Matter **23**, 013001 (2011).

[16] P. Hohenberg and W. Kohn, Phys. Rev. **136**, B864 (1964).

[17] T. Ono, M. Heide, N. Atodiresei, P. Baumeister, S. Tsukamoto, and S. Blügel, Phys. Rev. B **82**, 205115 (2010); T. Ono and K. Hirose, *ibid.* **72**, 085115 (2005); K. Hirose, T. Ono, Y. Fujimoto, and S. Tsukamoto, *First-Principles Calculations in Real-Space Formalism* (Imperial College Press, London, 2005).

[18] J. R. Chelikowsky, N. Troullier, and Y. Saad, Phys. Rev. Lett. **72**, 1240 (1994); J. R. Chelikowsky, N. Troullier, K. Wu, and Y. Saad, Phys. Rev. B **50**, 11355 (1994).

[19] P. E. Blöchl, Phys. Rev. B **50**, 17953 (1994).

[20] J. P. Perdew and A. Zunger, Phys. Rev. B **23**, 5048 (1981).

[21] T. Ono and K. Hirose, Phys. Rev. Lett. **82**, 5016 (1999).

[22] Y. Egami, K. Hirose, and T. Ono, Phys. Rev. E **82**, 056706 (2010); L. Kong, M. L. Tiago, and J. R. Chelikowsky, Phys. Rev. B **73**, 195118 (2006); T. Ono, S. Tsukamoto, Y. Egami, and Y. Fujimoto, J. Phys.: Condens. Matter **23**, 394203 (2011).

[23] L. Kong, J. R. Chelikowsky, J. B. Neaton, and S. G. Louie, Phys. Rev. B **76**, 235422 (2007).

[24] M. Büttiker, Y. Imry, R. Landauer, and S. Pinhas, Phys. Rev. B **31**, 6207 (1985).

[25] M. Brandbyge, M. R. Sørensen, and K. W. Jacobsen, Phys. Rev. B **56**, 14956 (1997); N. Kobayashi and M. Tsukada, Jpn. J. Appl. Phys. **38**, 3805 (1999).

[26] M. Strange, C. Rostgaard, H. Häkkinen, and K. S. Thygesen, Phys. Rev. B **83**, 115108 (2011); T. Rangel, A. Ferretti, P. E. Trevisanutto, V. Olevano, and G.-M. Rignanese, *ibid.* **84**, 045426 (2011).

[27] M. Bürkle, J. K. Viljas, D. Vonlanthen, A. Mishchenko, G. Schön, M. Mayor, T. Wandlowski, and F. Pauly, Phys. Rev. B **85**, 075417 (2012); D. J. Mowbray, G. Jones, and K. S. Thygesen, J. Chem. Phys. **128**, 111103 (2008).

[28] The O-O distance in a carboxylic acid group is almost commensurate with the Cu-Cu distance in the [$\bar{1}$10] direction of a Cu(110) surface. For further discussion, see N. Atodiresei, K. Schroeder, and S. Blügel, Phys. Rev. B **75**, 115407 (2007); B. G. Frederick,

R. J. Cole, J. R. Power, C. C. Perry, Q. Chen, N. V. Richardson, P. Weightman, C. Verdozzi, D. R. Jennison, P. A. Schultz, and M. P. Sears, *ibid.* **58**, 10883 (1998); M. Pascal, C. Lamont, M. Kittel, J. Hoeft, R. Terborg, M. Polcik, J. Kang, R. Toomes, and D. Woodruff, Surf. Sci. **492**, 285 (2001).

[29]In this work, we have used the theoretical lattice parameter of the Cu fcc crystal, 3.64 Å (6.87 bohrs).

[30]This approximation advantageously enables us to use an analytical function set to describe the boundary conditions, and is well known to give reasonable transport results, e.g., in Refs. 10 and 13, and also in K. Hirose, N. Kobayashi, and M. Tsukada, Phys. Rev. B **69**, 245412 (2004); M. Otani, T. Ono, and K. Hirose, *ibid.* **69**, 121408 (2004); M. Di Ventra and N. D. Lang, *ibid.* **65**, 045402 (2001).

[31]As the broadening function, we have used the Gaussian function, $f(E) = A \exp(-(\lambda E)^2)$ and $\lambda^{-1} = \sqrt{2} \cdot k_B T$. Here, A is the normalization constant as $A = \lambda/\sqrt{\pi}$, k_B is the Boltzmann constant, and T is temperature set to be 450 K in this work.

[32]N. Atodiresei, V. Caciuc, P. Lazić, and S. Blügel, Phys. Rev. Lett. **102**, 136809 (2009); G. D. Zeiss and M. A. Whitehead, J. Chem. Soc. A **1971**, 1727 (1971); I. Fleming, *Frontier Orbitals and Organic Chemical Reactions* (John Wiley & Sons, New York, 1976).

[33]P. Pyykkö and M. Atsumi, Chem. Eur. J. **15**, 186 (2009).